Research Article

Achieving Submicrosecond Thermally Activated Delayed Fluorescence Lifetime and Highly Efficient Electroluminescence by Fine-Tuning of the Phenoxazine–Pyrimidine Structure

Tomas Serevičius,* Rokas Skaisgiris, Jelena Dodonova, Laimis Jagintavičius, Dovydas Banevičius, Karolis Kazlauskas, Sigitas Tumkevičius, and Saulius Juršėnas

Cite This: ACS Appl. Mater. Interfaces 2020, 12, 10727–10736

Read Online

ACCESS | Metrics & More | Article Recommendations | Supporting Information

ABSTRACT: Thermally activated delayed fluorescence (TADF) materials, combining high fluorescence quantum efficiency and short delayed emission lifetime, are highly desirable for application in organic light-emitting diodes (OLEDs) with negligible external quantum efficiency (EQE) roll-off. Here, we present the pathway for shortening the TADF lifetime of highly emissive 4,6-bis[4-(10-phenoxazinyl)phenyl]pyrimidine derivatives. Tiny manipulation of the molecular structure with methyl groups was applied to tune the singlet–triplet energy-level scheme and the corresponding coupling strengths, enabling the boost of the reverse intersystem crossing (rISC) rate (from 0.7 to 6.5) $\times 10^6$ s^{-1} and shorten the TADF lifetime down to only 800 ns in toluene solutions. An almost identical TADF lifetime of roughly 860 ns was attained also in solid films for the compound with the most rapid TADF decay in toluene despite the presence of inevitable conformational disorder. Concomitantly, the boost of fluorescence quantum efficiency to near unity was achieved in solid films due to the weakened nonradiative decay. Exceptional EQE peak values of 26.3–29.1% together with adjustable emission wavelength in the range of 502–536 nm were achieved in TADF OLEDs. Reduction of EQE roll-off was demonstrated by lowering the TADF lifetime.

KEYWORDS: TADF, pyrimidine, phenoxazine, conformational disorder, rISC, OLEDs
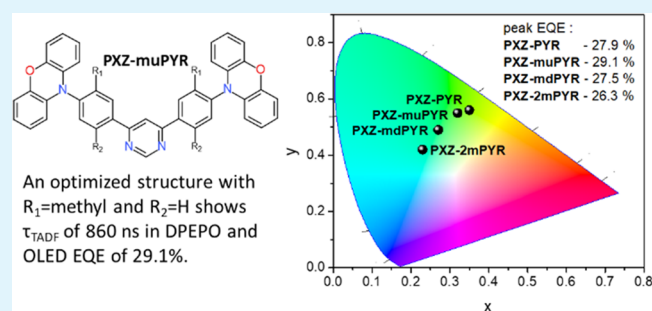
INTRODUCTION

Thermally activated delayed fluorescence (TADF) is an elegant way to employ the "dark" triplet states in organic light-emitting diode (OLED) devices and to achieve nearly 100% internal quantum efficiency[1,2] without the usage of expensive and rare heavy metals, for example, iridium.[3,4] The recent progress in design of TADF materials[5–7] and understanding the processes behind the reverse intersystem crossing (rISC)[8–15] led to the realization of green and sky-blue TADF OLEDs with external quantum efficiency (EQE) values approaching 40%.[16,17] However, large EQE values usually are demonstrated only at low luminance, and pronounced EQE roll-off at larger luminance usually is observed due to the emergence of triplet–triplet, singlet–triplet, and similar annihilation pathways.[18,19] Boosting the rISC rate has been shown to be the successful strategy for lowering the EQE roll-off;[19–21] however, shortening the TADF lifetime is rather a difficult task,[22,23] requiring the minimization of energy gaps between the coupled singlet and triplet states.[8,23] This is achieved by selecting the appropriate electron-donating (D) and electron-accepting (A) units and bounding them in an appropriate molecular geometry.[21] Among the wide variety of possible donor fragments, phenoxazine (PXZ) was shown to
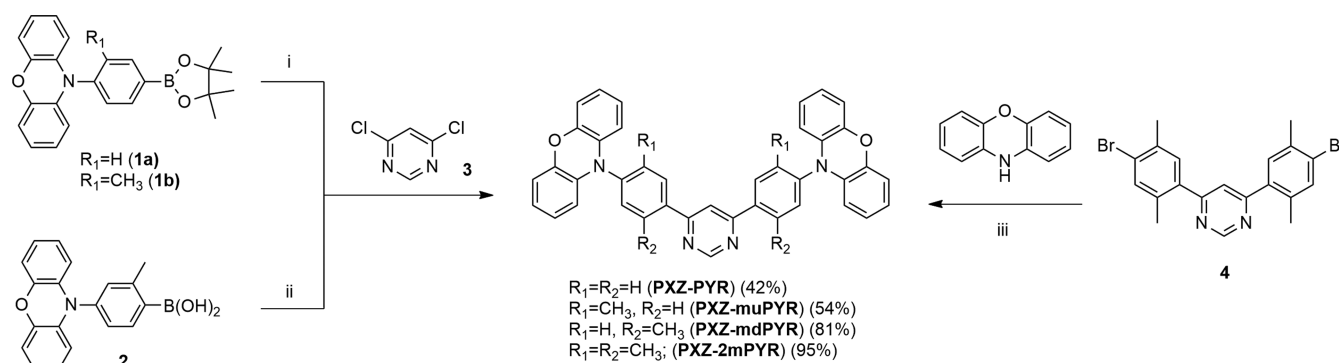
be a good candidate for achieving the short TADF lifetime together with a high fluorescence quantum yield[24–32] due to the strong enough electron-donating properties and ability to show large steric hindrance to acceptor units.[21,33] However, being noncontinuously conjugated, phenoxazine is found in two forms, planar and crooked conformation, and only the planar form shows strong TADF.[34,35] This issue can be solved by weakening the interaction between the phenoxazine and the electron-accepting part of the TADF molecule by introducing the spacer unit, minimizing the population of crooked conformations, and enhancing the number of TADF-active planar orientations.[28,36] The application of such molecular design by using phenoxazine D and suitable pyrimidine (PYR) electron-acceptor (A) together with phenyl spacer units (s) in a D-s-A-s-D layout allowed to achieve highly efficient single-band fluorescence with a TADF lifetime of 2.56 μs together with an EQE value of 19.9%.[24] The later modification of a

Scheme 1. Synthesis of 4,6-Bis[4-(10-phenoxazinyl)phenyl]pyrimidines PXZ-PYR, PXZ-muPYR, PXZ-mdPYR, and PXZ-2mPYR[a]

R₁=H (**1a**)
R₁=CH₃ (**1b**)

2

3

R₁=R₂=H (**PXZ-PYR**) (42%)
R₁=CH₃, R₂=H (**PXZ-muPYR**) (54%)
R₁=H, R₂=CH₃ (**PXZ-mdPYR**) (81%)
R₁=R₂=CH₃; (**PXZ-2mPYR**) (95%)

4

[a]Reagents and conditions: (i) boronic ester **1a** or **1b** (2.2 equiv), Pd(PPh₃)₄ (10 mol %), aq. K₂CO₃ (15 equiv), glyme, 80 °C, 24 h; (ii) boronic acid **2** (2.5 equiv), Pd(OAc)₂ (10 mol %), PPh₃ (20 mol %), aq. Na₂CO₃ (6.2 equiv), glyme, 90 °C, 24 h; (iii) phenoxazine (2.2 equiv), Pd₂dba₃ (5 mol %), P(t-Bu)₃·HBF₄ (10 mol %), NaOt-Bu (3 equiv), toluene, Ar, 110 °C, 24 h.

promising phenoxazine−pyrimidine structure by different aryl and methyl moieties at the pyrimidine unit resulted in subsequent lowering of the TADF decay time down to 1.99 μs while preserving a high emission yield.[24,25] Further substantial shortening of the TADF lifetime down to 1.32 μs for the analogous phenoxazine−pyrimidine compounds was achieved by introducing Cl or Br atoms and enhancing both ISC and rISC rates due to internal heavy-atom effect, simultaneously preserving a high fluorescence quantum yield. This strategy also allowed to increase peak EQE values up to 25.3%.[26] However, boosting the rISC rate by halogenation results in the redshift of the emission wavelength,[26,37,38] which is beneficiary while seeking the green-to-yellow emission, however other approaches are needed for blue TADF.

Inspired by the potential of pyrimidine−phenoxazine TADF compounds for achieving rapid and highly efficient TADF, we performed the further modification of the 4,6-bis[4-(10-phenoxazinyl)phenyl]pyrimidine molecular structure aiming the additional shortening of the TADF lifetime. Tiny alteration of the molecular structure was performed by inserting methyl units at the different positions of the phenylpyrimidine fragment, changing the geometry and rigidity of the molecular structure. The comprehensive analysis of time-resolved fluorescence spectra revealed the remarkable impact of methyl substitution pattern to energy-level alignment and fluorescence decay rate constants. An optimum molecular geometry was revealed with a balanced ratio between the singlet−triplet energy splittings and corresponding coupling strengths, showing the submicrosecond solid-state TADF lifetime and high emission yield. The optimized TADF compounds were employed in optimized OLED devices as emitters with tunable emission color. Outstanding peak EQE values of 26.3−29.1% were obtained with minimized EQE roll-off.

EXPERIMENTAL SECTION

Reagents and solvents were purchased directly from commercial suppliers; solvents were purified by known procedures. Melting points were determined in open capillaries with a digital melting point IA9100 series apparatus (Thermo Fisher Scientific) and were not corrected. Thin layer chromatography was performed using TLC aluminum sheets with silica gel (Merck 60 F254). Visualization was accomplished by UV light. Column chromatography was performed using silica gel 60 (0.040−0.063 mm) (Merck). NMR spectra were recorded on a Bruker Ascend 400 (400 and 100 MHz for ¹H and ¹³C,

respectively). ¹H NMR and ¹³C NMR spectra were referenced to residual solvent peaks. High-resolution mass spectrometry (HRMS) analyses were carried out on microTOF-Q II or microTOF-Q III mass spectrometers (Bruker). DSC curves were measured by Mettler Toledo DSC1 apparatus using aluminum crucibles under N₂ flow. Sample mass was around 8−10 mg, and heating and cooling rates were 10 K/min. TADF compounds were analyzed in 1 × 10⁻⁵ M toluene solutions, 1 wt % PMMA, and 10 wt % DPEPO films. Solid-state films were prepared by dissolving each material and host at appropriate ratios in toluene solutions and then wet-casting the solutions on quartz substrates. Absorption spectra were measured using a Lambda 950 UV/Vis spectrophotometer (PerkinElmer). Time-integrated fluorescence spectra (TIFL), time-resolved fluorescence spectra (TRFL), phosphorescence spectra and fluorescence decay transients were measured using a nanosecond YAG:Nd³⁺ laser NT 242 (Ekspla, τ = 7 ns, pulse energy 200 μJ, λ_ex = 300 nm, repetition rate = 1 kHz) and time-gated iCCD camera New iStar DH340T (Andor). Fluorescence transients were obtained by exponentially increasing delay and integration time. This allows to record up to 10 orders of magnitude in time and intensity of the fluorescence decay.[39] Fluorescence quantum yields (Φ_F) within the ±5% error of the solutions and polymer films in ambient air were estimated by the integrated sphere method[40] using an integrating sphere (Sphere Optics) connected to the CCD spectrometer PMA-12 (Hamamatsu) via optical fiber. Solid-state samples were mounted in a closed-cycle He cryostat (Cryo Industries 204 N) for all measurements (for oxygen-saturated (+O₂) and oxygen-free (−O₂) conditions). Toluene solutions were degassed by using the freeze−pump−thaw method. OLED devices were fabricated on precleaned indium-tin oxide (ITO)-coated glass substrates. The small-molecule and cathode layers were thermally evaporated using a vacuum evaporation apparatus (Vacuum Systems and Technologies Ltd) at <6 × 10⁻⁶ Torr pressure and deposition rate of about 1 Å/s. OLED devices were encapsulated with a clear glass cover to prevent the interaction with ambient atmosphere. Device current−voltage (I−V) characteristics and electroluminescence properties were measured using a calibrated integrating sphere (Orb Optronics) and CCD spectrometer PMA-11 (Hamamatsu), powered by a 2601A power supply unit (Keithley).

RESULTS AND DISCUSSION

Molecular Design. Four TADF compounds, bearing phenoxazine electron-donor and diphenylpyrimidine electron-acceptor units, were synthesized and comprehensively analyzed. 4,6-Bis[4-(10-phenoxazinyl)phenyl]pyrimidine (**PXZ-PYR**) was taken as a starting point for further optimization due to the high solid-state fluorescence efficiency
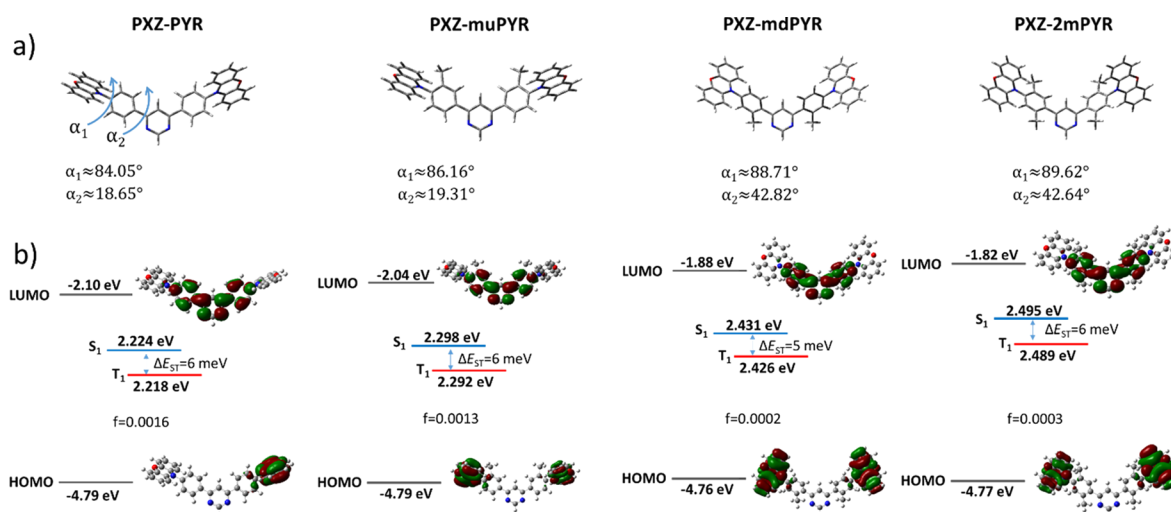
Figure 1. (a) DFT-optimized molecular geometries of TADF compounds **PXZ-PYR**, **PXZ-muPYR**, **PXZ-mdPYR**, and **PXZ-2mPYR**. α_1 and α_2 are dihedral angles between phenyl−phenoxazine and phenyl−pyrimidine units, respectively. (b) HOMO and LUMO energies, $S_0 \rightarrow S_1/T_1$ absorption energies with corresponding transition oscillator strengths and $S_1 - T_1$ energy gaps (ΔE_{ST}) and π-electron density distribution in the HOMO and LUMO of compounds **PXZ-PYR**, **PXZ-muPYR**, **PXZ-mdPYR**, and **PXZ-2mPYR**.

(0.88) and rapid TADF decay (2.56 μs).[24] Various modifications of the **PXZ-PYR** structure were demonstrated,[24,26] seeking for the shortening of the TADF lifetime; however, either the effect was rather low (from 2.56 to 1.99 μs[24]) or the modification resulted in usually unwanted narrowing of the bandgap.[26] As a solution, molecular structure modification of similar D-s-A-s-D TADF compounds bearing acridine donor units by methyl units for the minimization of τ_{TADF} without the emission redshift was suggested by Komatsu et al.[41] The presented strategy allowed to widen the energy gap and observe the blueshift of the emission peak. Such a strategy was also successfully applied for different TADF compounds.[42−46] Inspired by such observations and our previous findings,[37] we designed three new phenoxazine−pyrimidine TADF compounds with methyl units introduced into the acceptor unit. In contrast to Komatsu et al.,[41] we tuned the twist angles not only between the pyrimidine and phenyl units but also between the phenyl units and phenoxazine, seeking for more pronounced alteration of TADF properties and a molecular rigidity increase. Namely, compound **PXZ-muPYR** was modified with *meta*-methyl units, **PXZ-mdPYR** by *ortho*-methyl moieties, and **PXZ-2mPYR** by both *meta*- and *ortho*-methyl units at the phenyl spacers (see Scheme 1).

Synthesis and Thermal Properties. Synthetic routes of the designed molecules **PXZ-PYR**, **PXZ-mdPYR**, **PXZ-muPYR**, and **PXZ-2mPYR** are outlined in Scheme 1. 4,6-Bis[4-(10-phenoxazinyl)phenyl]pyrimidine (**PXZ-PYR**)[24] and 4,6-bis[3-methyl-4-(10-phenoxazinyl)phenyl]pyrimidine (**PXZ-muPYR**) were synthesized by the Suzuki−Miyaura cross-coupling reaction of 4,6-dichloropyrimidine (**3**) with corresponding 4-(10-pheoxazinyl)phenyl boronates (**1a,b**) in the presence of Pd(PPh$_3$)$_4$ as a catalyst. Coupling of boronic acid **2** with 4,6-dichloropyrimidine (**3**) using Pd(OAc)$_2$/PPh$_3$ as a catalyst system gave **PXZ-mdPYR** in a good yield (81%). Compound **PXZ-2mPYR** bearing two methyl groups in a phenyl spacer between pyrimidine and phenoxazine moieties was obtained in an excellent yield (95%) by reacting 4,6-bis(4-bromo-2,5-dimethylphenyl)pyrimidine (**4**), previously reported by us,[37] with phenoxazine under the palladium-

catalyzed amination reaction conditions. For clarity, methyl groups in the phenyl spacer will be hereinafter referred to as follows: 2-methyl group in compounds **PXZ-mdPYR** and **PXZ-2mPYR** as *ortho*-methyl group and 3-methyl group in **PXZ-muPYR** and 5-methyl group in **PXZ-2mPYR** as *meta*-methyl groups. The synthetic details and characterization data of the synthesized 4-(10-phenoxazinyl)phenylboronic acid esters **1a,b**, boronic acid **2**, and target compounds **PXZ-PYR**, **PXZ-muPYR**, **PXZ-muPYR**, and **PXZ-2mPYR** are presented in the Supporting Information.

Differential scanning calorimetry analysis (see Figure S21 in the Supporting Information) revealed that all phenoxazine−pyrimidine compounds were molecular glasses with glass transition temperatures ranging from 109 to 137 °C, typically for similar phenoxazine−pyrimidine TADF materials.[24,26]

DFT Simulations. Quantum chemical calculations were performed by using density functional theory (DFT) as implemented in the Gaussian 09 software package at the B3LYP/6-31G(d) level.[47] Polarizable continuum model (PCM) was used to estimate the solvation behavior of the toluene surrounding.

The synthesized phenoxazine−pyrimidine TADF compounds **PXZ-PYR**, **PXZ-muPYR**, **PXZ-mdPYR**, and **PXZ-2mPYR** were optimized at the ground-state molecular geometry and π-electron density distribution in the HOMO and LUMO, and $S_0 \rightarrow S_1/T_1$ transition energies with corresponding oscillator strengths were calculated (see Figure 1). DFT analysis revealed that the lowest-energy molecular conformations were those with a planar (quasi-equatorial) orientation of the PXZ unit[28,34] (see Figure S22 in the Supporting Information for the detailed analysis). The phenoxazine fragment was nearly perpendicular in all compounds with minor variations of the twist angle (angle α_1 in Figure 1). The modification of the molecular structure with *ortho*-methyl groups had a pronounced effect on the twist angle between phenyl and pyrimidine units (angle α_2 in Figure 1). Both phenyls were weakly twisted with respect to the pyrimidine fragment in **PXZ-PYR** and **PXZ-muPYR**; however, α_2 angle increased from about 19° to nearly 43° after the introduction of the *ortho*-methyl group due to the enhanced

steric hindrance. It had an evident effect on the energies of LUMO, which increased from about −2.04 to −2.10 eV for compounds **PXZ-PYR** and **PXZ-muPYR**, respectively, and from −1.82 to −1.88 eV for compounds **PXZ-mdPYR** and **PXZ-2mPYR**, respectively, weakening the electron-accepting ability and enlarging the bandgap, while the HOMO energies were almost the same (from −4.76 to −4.79 eV). All phenoxazine−pyrimidine compounds showed charge-transfer (CT) character when the electron density in the HOMO mostly was distributed over the phenoxazine unit, while in the LUMO, the π-electron density was localized over the diphenylpyrimidine moiety. Molecular structure modification also had the pronounced effect on singlet and triplet transition energies and the corresponding oscillator strengths. $S_0 \rightarrow S_1$ transition energies ranged at 2.224−2.298 eV for **PXZ-PYR** and **PXZ-muPYR** with an oscillator strength of 0.0013−0.0016. The enlarged $S_0 \rightarrow S_1$ transition energies up to about 2.495 eV with an oscillator strength of 0.0002−0.0003 were observed for *ortho*-methyl modified compounds **PXZ-mdPYR** and **PXZ-2mPYR** with the lowest electron cloud overlap in the HOMO and LUMO and the weakest electron-acceptor. The same trend was also estimated for $S_0 \rightarrow T_1$ transition, when the transition energies of <2.3 eV were estimated for compounds **PXZ-PYR** and **PXZ-muPYR** and >2.4 eV for **PXZ-mdPYR** and **PXZ-2mPYR** with corresponding singlet−triplet gaps of only 5−6 meV. Such a negligible splitting shows the possibility of highly efficient TADF with controllable emission properties.

Absorption and Emission Properties. The impact of molecular core modifications for absorption and fluorescence properties of phenoxazine−pyrimidine compounds was revealed by analyzing absorption and emission spectra in toluene solutions (see Figure 2 and Table 1).
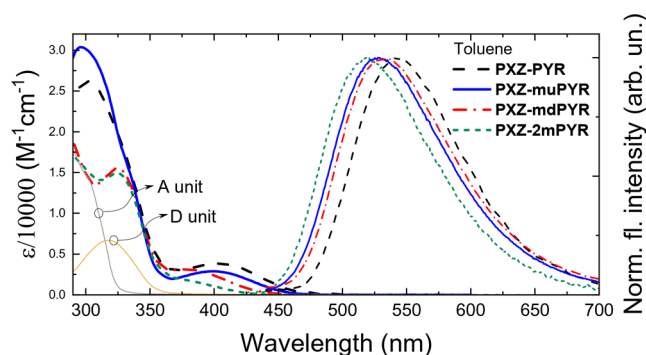

Figure 2. Absorption and fluorescence spectra of compounds **PXZ-PYR**, **PXZ-muPYR**, **PXZ-mdPYR**, and **PXZ-2mPYR** in toluene. Absorption spectra of diphenylpyrimidine A and phenoxazine D units are also shown.

Two regions can be discerned in the absorption spectra, peaking at about 300−320 and 380−400 nm (with absorption tail until about 500 nm). The absorption peaks at the higher energies were the composition of the absorption of individual phenoxazine and phenylpyrimidine units. Since no absorption of donor or acceptor units extended beyond ∼375 nm, the lower energy absorption band was attributed to the absorption of charge-transfer states.[24,26,28] Larger molar absorption values (up to about 3900 M^{-1} cm^{-1}) were observed for compounds **PXZ-PYR** and **PXZ-muPYR**, in line with DFT predictions. Fluorescence spectra of compounds **PXZ-PYR**, **PXZ-muPYR**, **PXZ-mdPYR**, and **PXZ-2mPYR** peaked at 519−543 nm in toluene solutions, typically for phenoxazine-based TADF compounds.[24−29] The introduction of methyl groups into the phenyl spacer unit allowed us to tune the CT emission wavelength for 100 meV when the fluorescence of the unmodified **PXZ-PYR** peaked at 543 nm and blueshifted up to 519 nm for **PXZ-2mPYR**. This was achieved by the manipulating the electron density overlap in the HOMO and LUMO and the strength of donor unit, as shown by DFT calculations. Fluorescence quantum yields (Φ_F) of TADF compounds in toluene solutions ranged from 0.1 to 0.15 and were larger for compounds without the *meta*-methyl fragments (see Table 1).

To reveal the nature of Φ_F variation, radiative (k_r) and nonradiative (k_{nr}) fluorescence decay rates of phenoxazine−pyrimidine compounds were estimated (see Table 1). Compounds **PXZ-PYR** and **PXZ-muPYR** with the largest oscillator strength showed the most rapid radiative decay; however, k_r was almost twice lower for **PXZ-muPYR**, resulting in Φ_F decrease. Simultaneously, both **PXZ-PYR** and **PXZ-muPYR** with the most flexible molecular structure showed the fastest nonradiative decay due to the pronounced excited-state relaxation (and/or, probably, different ISC rates), though the introduction of the *meta*-methyl unit lowered the nonradiative decay for about 17%. The further modification of the molecular structure with *ortho*-methyl units weakened the HOMO−LUMO overlap and lowered the radiative decay rate. Despite that, compounds **PXZ-mdPYR** and **PXZ-2mPYR** benefited from the more rigid molecular structure, leading to about 60% lowered nonradiative decay rate.[48,49] The weaker nonradiative decay, despite the lowered radiative decay rate, resulted in enhanced Φ_F for compound **PXZ-mdPYR**, almost the same as for **PXZ-PYR** with the largest k_r.

The nonradiative decay was further suppressed by embedding phenoxazine−pyrimidine compounds in solid polymer films. In this case, the emission peaked at 498−513 nm, slightly blueshifted with respect to toluene solutions due to weaker solid-state solvation in the PMMA surrounding[50] (see Figure S23 in the Supporting Information). Same as in

Table 1. Absorption and Emission Data of Compounds PXZ-PYR, PXZ-muPYR, PXZ-mdPYR, and PXZ-2mPYR in Toluene Solutions

compounds	λ_{ABS} (nm)[a]	ε (M^{-1} cm^{-1})[b]	λ_{FL} (nm)[c]	Φ_F[d]	k_{FL} ($\times 10^7$ s^{-1})[e]	k_r ($\times 10^6$ s^{-1})[f]	k_{nr} ($\times 10^7$ s^{-1})[g]
PXZ-PYR	402	3880	543	0.15	7.5	11.3	6.4
PXZ-muPYR	401	2880	530	0.1	6.1	6.1	5.5
PXZ-mdPYR	375	3100	528	0.14	4.0	5.6	3.4
PXZ-2mPYR	-*	below 2000*	519	0.1	4.2	4.2	3.8

[a]Peak wavelength of the lowest energy absorption band. *, no clear absorption peak. [b]Molar absorption coefficient of the lowest energy absorption band. *, approximate value. [c]Peak wavelength of the fluorescence spectrum. [d]Fluorescence quantum yield. [e]Fluorescence decay rate. [f]Radiative fluorescence decay rate ($k_{FL} \times \Phi_{FL}$). [g]Nonradiative fluorescence decay rate ($k_{FL} \times (1 - \Phi_{FL})$).

toluene, unmodified **PXZ-PYR** peaked at the longest wavelengths, while compounds modified with *ortho*-methyl units peaked at the shortest wavelengths. Fluorescence quantum yields of compounds in PMMA films were enhanced due to the largely minimized nonradiative decay. Φ_F were 0.26, 0.16, 0.19, and 0.13 for **PXZ-PYR**, **PXZ-muPYR**, **PXZ-mdPYR**, and **PXZ-2mPYR**, respectively (see Figure S24 in the Supporting Information for the estimation of Φ_F for polymer films). A more pronounced increase in Φ_F was estimated for less rigid compounds.

Phosphorescence (PH) properties of phenoxazine–pyrimidine compounds were investigated by analyzing low-temperature spectra of 1 wt % PMMA films (see Figure 3). Clear
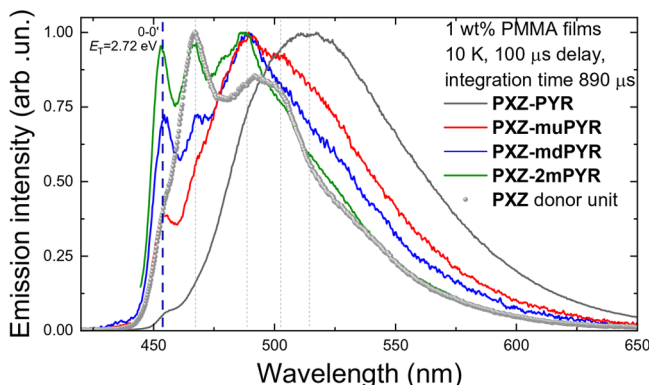

Figure 3. Normalized emission spectra of 1 wt % PMMA films of compounds **PXZ-PYR**, **PXZ-muPYR**, **PXZ-mdPYR**, and **PXZ-2mPYR** and the phenoxazine (**PXZ**) donor unit at 10 K. Spectra were obtained after 100 μs delay with 890 μs integration time.

vibronic progression was observed, typically for localized-excited state (^{3}LE) emission. Vibronic bands of more rigid compounds **PXZ-muPYR**, **PXZ-mdPYR**, and **PXZ-2mPYR** peaked at the same wavelengths as that of the phenoxazine donor fragment, and the intensity of the 0th vibronic band was the largest for the most rigid **PXZ-2mPYR**, indicating negligible reorganization of the molecular structure in the excited state. On the other hand, those strongly overlapped and broadened lower energy vibronic bands clearly dominated in the phosphorescence spectrum of the least sterically constrained **PXZ-PYR**, though the weak 0th vibronic band still was visible. Therefore, all phosphorescence spectra originate from the phenoxazine electron-donor unit with the same T_1 energy of 2.72 eV. These results contradicts with other reports of similar D-s-A-s-D phenoxazine–pyrimidine materials and even the report of same compound **PXZ-PYR**[24] when the T_1 states were shown to be at the lower energies.[24−26] The estimated singlet–triplet energy gaps of phenoxazine–pyrimidine compounds in PMMA films (calculated by subtracting the energy of phosphorescence's 0th vibronic peak from the onset energy of fluorescence spectra) were in the range of 10−150 meV (10, 70, 150, and 130 meV for **PXZ-PYR**, **PXZ-muPYR**, **PXZ-mdPYR**, and **PXZ-2mPYR**, respectively; see Figure S25 in the Supporting Information). The lowest ΔE_{ST} was estimated for compounds **PXZ-PYR** and **PXZ-muPYR**, while the compounds with the lowered HOMO−LUMO overlap showed enlarged ΔE_{ST}.

To sum up, the introduction of methyl groups to the bridging phenyl unit enabled the significant reduction of k_{nr}; however, it also decreased k_r and enlarged the singlet−triplet

energy gaps. Later, it will be shown to have the crucial impact to TADF properties.

TADF Properties. In this section, solution and solid-state TADF properties of phenoxazine−phenylpyrimidine compounds will be discussed. All materials showed delayed fluorescence of TADF nature in both toluene solutions and PMMA films, as demonstrated by its temperature activation (see Figure S26 in the Supporting Information) and quenching by molecular oxygen (see Figures S27 and S28 in the Supporting Information). The fluorescence intensity of toluene solutions was strongly enhanced upon the oxygen removal for compounds **PXZ-muPYR** and **PXZ-2mPYR** (for 5.2−5.3 times), while for **PXZ-PYR** and **PXZ-mdPYR**, the enhancement was lower (for 2.7−2.8 times). Although Φ_F was rather similar for all compounds in $-O_2$ toluene (0.38−0.53), fluorescence quantum yields of delayed fluorescence (Φ_{DF}) were markedly larger for **PXZ-muPYR** and **PXZ-2mPYR** than those for **PXZ-PYR** and **PXZ-mdPYR** (~0.42 vs ~0.25), together with remarkably enhanced DF/PF ratios (~4.3 vs ~1.8).

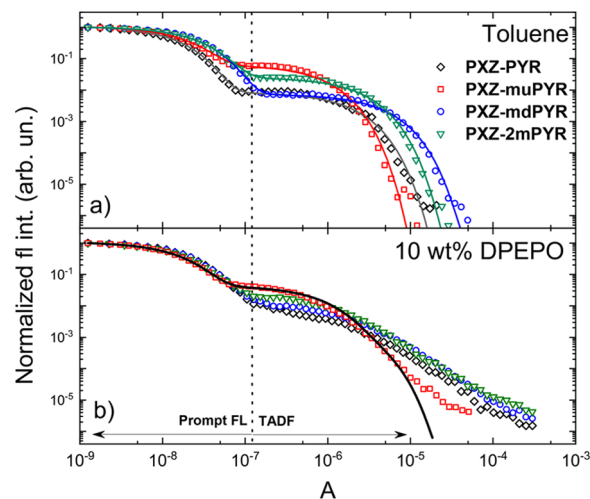The TADF lifetime of phenoxazine−pyrimidine compounds in toluene solutions (see Figure 4a and Table 2) was rather fast

Figure 4. Normalized fluorescence decay transients of phenoxazine−pyrimidine TADF compounds in (a) $-O_2$ toluene and (b) 10 wt % DPEPO films. Color lines are biexponential fits, while the black line in (b) is a triexponential fit.

for compounds **PXZ-PYR**, **PXZ-mdPYR**, and **PXZ-2mPYR** with the lifetime ranging from 1.6 to 4.0 μs, while for **PXZ-muPYR**, the TADF decay time decreased down to 0.8 μs. This value was among the lowest reported for solutions,[20,22,28,38,51] though the low TADF lifetime in solutions with Φ_F of only ~0.5 could also be affected by the nonradiative fluorescence recombination.[52] Clearly, the molecular structure had a direct effect on TADF properties, altering the rates of ISC and rISC in toluene solutions (see Table 2). According to Gibson et al.,[8] efficient ISC and rISC require the combination of large spin-orbit coupling between ^{1}CT and ^{3}LE states and large vibronic coupling between ^{3}LE and ^{3}CT states (via the torsion of D-A angle), together with small corresponding energy gaps (^{1}CT-^{3}LE and ^{3}LE-^{3}CT, respectively).

In our case, we obviously tune the rotational flexibility of PXZ unit and alter the ^{1}CT-^{3}LE gap by changing the HOMO−LUMO overlap. Likewise, ^{3}LE-^{3}CT gaps may also be different,

Table 2. TADF Properties of Compounds PXZ-PYR, PXZ-muPYR, PXZ-mdPYR, and PXZ-2mPYR in −O$_2$ Toluene[a]

compounds	Φ_F[b]	$\dfrac{DF}{PF}$[c]	Φ_{ISC}[d]	τ_{PF} (ns)[e]	τ_{TADF} (μs)[f]	k_{IC} (10^6 s^{-1})[g]	k_{ISC} (10^7 s^{-1})[h]	k_{rISC} (10^6 s^{-1})[i]
PXZ-PYR	0.15/0.27/0.42	1.8	0.64	13.3	1.6	16.0	4.8	1.8
PXZ-muPYR	0.1/0.42/0.52	4.2	0.81	16.4	0.8	5.6	4.9	6.5
PXZ-mdPYR	0.14/0.24/0.38	1.7	0.63	25.0	4.0	9.2	2.5	0.7
PXZ-2mPYR	0.1/0.43/0.53	4.3	0.81	23.8	2.1	3.7	3.4	2.5

[a]Calculations were carried out according to Dias et.al.[55] [b]Fluorescence quantum yield of prompt, delayed, and total fluorescence, respectively. [c]Delayed fluorescence/prompt fluorescence intensity ratio. [d]Triplet yield. It was estimated according to ref 53 using PH lifetime from Figure S29 in the Supporting Information. [e]Fluorescence decay time. [f]TADF decay time. [g]Internal conversion rate. [h]Intersystem crossing rate. [i]Reverse intersystem crossing rate. Alike k_{rISC} values, we also obtained accordingly to the model for compounds with $k_r \approx k_{rISC}$; see Table S1 in the Supporting Information.

while the spin-orbit coupling constants should be similar for compounds with a similar molecular structure.[53] All this resulted in changes of the ISC rate (from 4.8 to 4.9) × 10^7 s^{-1} for compounds PXZ-PYR and PXZ-muPYR, respectively, and (from 2.5 to 3.4) × 10^7 s^{-1} for PXZ-mdPYR and PXZ-2mPYR, respectively, together with more pronounced variation of the rISC rate from 6.5 × 10^6 s^{-1} (for PXZ-muPYR) to 0.7 × 10^6 s^{-1} (PXZ-mdPYR). Both rates were clearly lower for compounds with larger ^{1}CT-^{3}LE splittings but the same rotational flexibility of PXZ unit (e.g., PXZ-PYR vs PXZ-mdPYR and PXZ-muPYR vs PXZ-2mPYR). Here, the decrease in ISC and rISC rates mostly was caused by the enhancement of ^{1}CT-^{3}LE gaps. Surprisingly, the increase in both rates was found for compounds with more sterically constrained PXZ units, lowered IC rates, and, supposedly, weakened vibronic coupling between ^{3}LE and ^{3}CT states[54] (PXZ-PYR vs PXZ-muPYR and PXZ-mdPYR vs PXZ-2mPYR). In this case, the decrease in ^{3}LE-^{3}CT gaps for *meta*-methyl modified compounds PXZ-muPYR and PXZ-2mPYR probably was the cause of enhanced ISC and rISC rates,[11] though the exact mechanism still is debatable. The largest rISC rate (6.5 × 10^{-6} s^{-1}) and, therefore, the most rapid TADF decay (0.8 μs) was estimated for PXZ-muPYR together with one of the largest Φ_{TADF} (0.42) due to the largest k_{rISC}/k_{IC} ratio. On the other hand, the weakened IC rate for PXZ-2mPYR allowed us to achieve the same TADF quantum yield together with a large enough rISC rate of 2.5 × 10^{-6} s^{-1} as for PXZ-muPYR having 45% more rapid radiative decay. However, the nonradiative decay still was strong for all compounds, resulting in Φ_F way below 1.

The boost of the fluorescence quantum yield was achieved by embedding the TADF compounds into the solid PMMA polymer matrix in −O$_2$ conditions. Although the rotational flexibility of the molecular structure already was reduced by the introduction of methyl groups, the additional suppression of structural relaxation in a more rigid surrounding eliminated the remaining nonradiative decay. Near-unity Φ_F were observed for compounds PXZ-PYR, PXZ-muPYR, and PXZ-mdPYR (0.92, 0.94, and 0.95, respectively). A somewhat lower Φ_F of 0.72 was estimated for PXZ-2mPYR with the largest ΔE_{ST}.[41] For further solid-state TADF analysis, small-molecule host DPEPO (bis(2-(diphenylphosphino)phenyl) ether oxide) was selected due to the large triplet energy and larger polarity.[56] Similar to those of PMMA Φ_F values were obtained for 10 wt % DPEPO (bis(2-(diphenylphosphino)phenyl) ether oxide) films, when, for example, a Φ_F of 0.84 was estimated for PXZ-muPYR, comparable to that in PMMA within the measurement error. The more polar DPEPO surrounding favored more pronounced stabilization of CT energies, though the emission

energies were slightly redshifted with respect to PMMA films (λ_{FL} = 515−542 nm; see Figure S30 in the Supporting Information).^{1}CT-^{3}LE gaps were also reduced to nearly zero for PXZ-PYR and PXZ-muPYR and 50−100 meV for PXZ-mdPYR and PXZ-2mPYR, respectively (see Figure S30 in the Supporting Information). Prompt fluorescence decay transients of 10 wt % DPEPO films of compounds PXZ-PYR, PXZ-muPYR, PXZ-mdPYR, and PXZ-2mPYR in the −O$_2$ surrounding (see Figure 4b) were similar to toluene solutions; however, the TADF decay was strongly multiexponential for compounds PXZ-muPYR, PXZ-mdPYR, and PXZ-2mPYR due to the presence of conformational disorder (see Figure S31 in the Supporting Information for time-resolved spectra, showing temporal shifts of the emission peak).[37,52,56−61] Although no exact TADF lifetime and decay rates could be estimated, still the slowest TADF decay could be attributed for PXZ-2mPYR. On the contrary, an approximate three-exponential fit of fluorescence decay transient was successfully applied for PXZ-muPYR with the most rapid rISC in toluene,[37] though the latest DF decay tail (from about 10^{-5} to about 10^{-4} s) still was impossible to fit. Roughly, a solid-state TADF lifetime of only 860 ns was obtained, being one of the lowest among the ever reported for various TADF compounds[7,21,51,62] and especially for pyrimidine derivatives (see Table S2 in the Supporting Information).

To sum up, molecular structure modification by small methyl units is a powerful strategy for tunning of TADF properties. Later, the enhanced TADF decay rate together with a large fluorescence quantum yield will be shown to be essential for achieving highly efficient electroluminescence with low EQE roll-off.

Electroluminescence Properties. At the final stage, electroluminescence properties of phenoxazine−pyrimidine compounds PXZ-PYR, PXZ-muPYR, PXZ-mdPYR, and PXZ-2mPYR were elucidated (see Figure 5 and Table 3). Typical for similar phenoxazine−pyrimidine TADF compounds OLED structure was used:[24−26] indium tin oxide (ITO)/1,1-bis[[di-4-tolylamino)phenyl]cyclohexane (TAPC) (30 nm)/4,4′,4″-tri(N-carbazolyl)triphenylamine (TCTA) (5 nm)/10 wt % TADF emitter:DPEPO (bis(2-(diphenylphosphino)phenyl) ether oxide) (15 nm)/1,3,5-tri(m-pyridin-3-yl-phenyl)benzene (TmPyPB) (65 nm)/lithium fluoride (LiF) (0.8 nm)/Al (100 nm). However, contrary to the reports of similar phenoxazine−pyrimidine compounds,[24−26] the high triplet energy host DPEPO (E_T = 3.3 eV[25]) was used rather than CBP with lower triplet energy (E_T = 2.6 eV[25]) to efficiently confine triplet excitons (T$_1$ = 2.72 eV) in the emissive layer. Neighboring compounds TCTA and
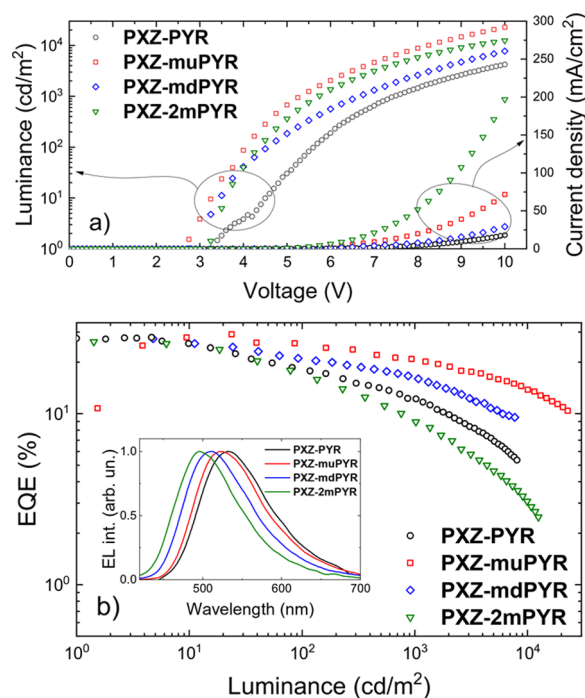
Figure 5. (a) Voltage−current density and voltage−luminance curves of the OLEDs. (b) External quantum efficiency dependence on the luminance of the OLEDs. Inset: electroluminescence spectra of devices at a driving voltage of 9 V.

TmPyPB were also selected to have larger T_1 energies than of emitting compounds to assist the exciton confinement.[63,64]

Electroluminescence (EL) spectra of all OLED devices (see the inset in Figure 5b) showed the emission only from the TADF emitter with no additional peaks from the host or neighboring materials. EL spectra peaked in the range of 502−536 nm. The alteration of the molecular structure allowed us to tune the EL peak wavelength from green, peaking at 536 nm for **PXZ-PYR** (CIE color coordinates of (0.35, 0.56)) to cyan for **PXZ-2mPYR**, peaking at 502 nm (CIE color coordinates of (0.23, 0.42)). EL turn-on voltages were in the range of 2.5−3.3 V, typically for OLEDs with a weakly electroactive DPEPO host.[65,66] The estimated peak values of power efficiency and luminance were in the range of 53.3−84.1 lm/W and 4214−22,730 cd/m². Very high external quantum efficiency (EQE) values were obtained, being among the highest values for pyrimidine compounds (see Table S3 in the Supporting Information). Compound **PXZ-muPYR** with the most rapid rISC and near-unity fluorescence quantum yield showed a peak EQE of 29.1% for green electroluminescence without introducing any outcoupling enhancement technique, con-

sistent with high Φ_F values and considering a light extraction yield of 0.2−0.3[67] (though the presence of molecular alignment of rod-like molecules, enhancing the outcoupling, still is possible[59,68]). A weak EQE roll-off of about 30% was observed when the EQE decreased down to 20.5% at the practical luminance of 1000 cd/m². A low EQE roll-off was achieved due to the short TADF lifetime of only 860 ns, weakening the EQE quenching by triplet−triplet and singlet−triplet annihilation at high luminance.[19,20] The combination of submicrosecond solid-state TADF lifetime and near 30% OLED EQE puts compound **PXZ-muPYR** among the most efficient TADF emitters (see Table S3 in the Supporting Information). Further optimization of EQE roll-off probably could be achieved by selecting a high T_1 host layer with larger carrier drift mobilities.[69] Also, very large EQE values were obtained for compounds **PXZ-PYR** and **PXZ-mdPYR** with similar near-unity Φ_F values, reaching 27.9 and 27.5%, respectively, though EQE roll-off was markedly larger due to the slower TADF decay. The lowest, though still large, peak EQE of 26.3% of cyan EL was estimated for compound **PXZ-2mPYR** with the lowest solid-state Φ_F; however, the EQE roll-off was rather large (an EQE of 8.9% at the luminance of 1000 cd/m²) due to the largest TADF lifetime. Therefore, all the OLEDs with phenoxazine−phenylpyrimidine TADF emitters showed high EQE values, ranging from 26.3 to 29.1%, differing mainly by EQE roll-off, which was determined by the TADF lifetime.

■ CONCLUSIONS

In summary, we presented the synthesis, comprehensive analysis, and device application of a series of TADF compounds based on the phenoxazine−phenylpyrimidine structure with high TADF efficiency and rapid delayed fluorescence decay. The modification of the molecular structure with methyl groups at the acceptor unit was employed to tune the acceptor properties and donor−acceptor interaction, which were shown to have a significant effect on emission properties of TADF compounds. First, the introduction of *ortho*-methyl units was found to reduce the acceptor strength, resulting in enlarged ¹CT-³LE energy gap and lowered rISC rate together with lowered TADF efficiency. On the contrary, the modification of the molecular structure with *meta*-methyl fragments was shown to be beneficial for enhancing the rISC rate up to $6.5 \times 10^6 \text{ s}^{-1}$ and shortening the TADF lifetime to 800 ns in toluene solutions. Lowering the ³LE-³CT energy gap was attributed as the nature of TADF enhancement. The modification of the phenoxazine−phenylpyrimidine molecular structure by introduction of both *ortho*- and *meta*-methyl units into the phenyl moiety was shown to lower the rISC rate and prolong TADF lifetime due to the

Table 3. Electroluminescence Properties of Phenoxazine−Pyrimidine TADF Compounds PXZ-PYR, PXZ-muPYR, PXZ-mdPYR, and PXZ-2mPYR

compounds	λ_{EL} (nm)[a]	V_{ON} (V)[b]	EQE[c]	PE_{MAX} (lm/w)[d]	L_{MAX} (cd/m²)[e]	CIE (x, y)[f]
PXZ-PYR	536	3.3	27.9/18.0/12.3	84.1	4214	(0.35, 0.56)
PXZ-muPYR	529	2.7	29.1/25.0/20.5	74.1	22730	(0.32, 0.55)
PXZ-mdPYR	514	2.5	27.5/21.0/16.0	75.2	7702	(0.27, 0.49)
PXZ-2mPYR	502	2.9	26.3/16.9/8.9	53.3	12476	(0.23, 0.42)

[a]Electroluminescence peak wavelength. [b]Electroluminescence turn-on voltage. [c]External quantum yield. The order of measured values: maximum/at 100 cd/m²/at 1000 cd/m². [d]Peak values of power efficiency. [e]Peak values of luminance. [f]Commission Internationale de l'Eclairage coordinates recorded at 9 V.

enlarged ^{1}CT-^{3}LE energy gap; however, the weakened IC rate allowed us to achieve a very large TADF quantum yield. An enhanced fluorescence quantum yield, reaching near unity, was achieved after the insertion of compounds in solid films and elimination of remaining nonradiative decay, though the solid-state Φ_F was slightly lower for compounds with both *ortho*- and *meta*-methyl units. Despite the Φ_F enhancement, the unwanted conformational disorder appeared in solid films, resulting in multiexponential TADF decay transients, though the TADF decay of the *meta*-methyl modified compound was successfully approximated with the three-exponential model, and a decay time of only about 860 ns was estimated, being one of the lowest reported for TADF compounds. Although no solid-state TADF lifetime was possible to evaluate for the rest of compounds, still it was evident that the slowest decay was for the compound with both methyl units. Highly efficient green electroluminescence with weak EQE roll-off was obtained when the external quantum efficiency of OLEDs made of the compound with the shortest TADF lifetime peaked at 29.1%, and an EQE of 20.5% was observed at a practical luminance of 1000 cd/m^2. Slightly lower peak EQE values of 27.1−27.5% with more pronounced EQE roll-off were obtained for compounds with slower TADF decay. Cyan EL with peak EQE of 26.3% was observed for *ortho*- and *meta*-methyl modified compounds with the shortest conjugation length, though the EQE roll-off was rather large due to the prolonged TADF decay.

Our results show that the fine-tuning of the TADF emitter structure by methyl groups enable the adjustment of the rISC rate, which directly controls the OLED performance at high current densities and enlarges the bandgap, which is favorable for the design of blue TADF emitters. Our insights, we believe, would be important for the optimization of TADF with compounds with diverse molecular structures.

ASSOCIATED CONTENT

Supporting Information
The Supporting Information is available free of charge at https://pubs.acs.org/doi/10.1021/acsami.9b21394.

Synthetic methods with NMR identification, DSC thermograms, DFT calculations of PXZ conformers, and detailed fluorescence properties (PDF)

AUTHOR INFORMATION

Corresponding Author
Tomas Serevičius − Institute of Photonics and Nanotechnology, Vilnius University, LT-10257 Vilnius, Lithuania; orcid.org/0000-0003-1319-7669; Email: tomas.serevicius@tmi.vu.lt

Authors
Rokas Skaisgiris − Institute of Photonics and Nanotechnology, Vilnius University, LT-10257 Vilnius, Lithuania
Jelena Dodonova − Institute of Chemistry, Vilnius University, LT-03225 Vilnius, Lithuania
Laimis Jagintavičius − Institute of Chemistry, Vilnius University, LT-03225 Vilnius, Lithuania
Dovydas Banevičius − Institute of Photonics and Nanotechnology, Vilnius University, LT-10257 Vilnius, Lithuania
Karolis Kazlauskas − Institute of Photonics and Nanotechnology, Vilnius University, LT-10257 Vilnius, Lithuania; orcid.org/0000-0001-7900-0465
Sigitas Tumkevičius − Institute of Chemistry, Vilnius University, LT-03225 Vilnius, Lithuania
Saulius Juršėnas − Institute of Photonics and Nanotechnology, Vilnius University, LT-10257 Vilnius, Lithuania

Complete contact information is available at:
https://pubs.acs.org/10.1021/acsami.9b21394

Author Contributions
The manuscript was written through contributions of all authors. All authors have given approval to the final version of the manuscript.

Notes
The authors declare no competing financial interest.

ACKNOWLEDGMENTS

REFERENCES

(1) Endo, A.; Ogasawara, M.; Takahashi, A.; Yokoyama, D.; Kato, Y.; Adachi, C. Thermally Activated Delayed Fluorescence from Sn4+-Porphyrin Complexes and Their Application to Organic Light Emitting Diodes - A Novel Mechanism for Electroluminescence. *Adv. Mater.* **2009**, *21*, 4802−4806.

(2) Uoyama, H.; Goushi, K.; Shizu, K.; Nomura, H.; Adachi, C. Highly Efficient Organic Light-Emitting Diodes from Delayed Fluorescence. *Nature* **2012**, *492*, 234−238.

(3) Baldo, M. A.; O'Brien, D. F.; You, Y.; Shoustikov, A.; Sibley, S.; Thompson, M. E.; Forrest, S. R. Highly Efficient Phosphorescent Emission from Organic Electroluminescent Devices. *Nature* **1998**, *395*, 151−154.

(4) Adachi, C.; Baldo, M. A.; Thompson, M. E.; Forrest, S. R. Nearly 100% Internal Phosphorescence Efficiency in an Organic Light-Emitting Device. *J. Appl. Phys.* **2001**, *90*, 5048.

(5) Wong, M. Y.; Zysman-Colman, E. Purely Organic Thermally Activated Delayed Fluorescence Materials for Organic Light-Emitting Diodes. *Adv. Mater.* **2017**, *29*, 1605444.

(6) Liang, X.; Tu, Z.-L.; Zheng, Y.-X. Thermally Activated Delayed Fluorescence Materials: Towards Realization of High Efficiency Through Strategic Small Molecular Design. *Chem. — Eur. J.* **2019**, *25*, 5623−5642.

(7) Konidena, R. K.; Lee, J. Y. Molecular Design Tactics for Highly Efficient Thermally Activated Delayed Fluorescence Emitters for Organic Light Emitting Diodes. *Chem. Rec.* **2019**, *19*, 1499−1517.

(8) Gibson, J.; Monkman, A. P.; Penfold, T. J. The Importance of Vibronic Coupling for Efficient Reverse Intersystem Crossing in Thermally Activated Delayed Fluorescence Molecules. *ChemPhysChem* **2016**, *17*, 2956−2961.

(9) Etherington, M. K.; Gibson, J.; Higginbotham, H. F.; Penfold, T. J.; Monkman, A. P. Revealing the Spin−Vibronic Coupling Mechanism of Thermally Activated Delayed Fluorescence. *Nat. Commun.* **2016**, *7*, 13680.

(10) Chen, X.-K.; Kim, D.; Brédas, J.-L. Thermally Activated Delayed Fluorescence (TADF) Path toward Efficient Electroluminescence in Purely Organic Materials: Molecular Level Insight. *Acc. Chem. Res.* **2018**, *51*, 2215−2224.

(11) Noda, H.; Nakanotani, H.; Adachi, C. Excited State Engineering for Efficient Reverse Intersystem Crossing. *Sci. Adv.* **2018**, *4*, eaao6910.

(12) Saigo, M.; Miyata, K.; Tanaka, S.; Nakanotani, H.; Adachi, C.; Onda, K. Suppression of Structural Change upon S$_1$ −T$_1$ Conversion

Assists the Thermally Activated Delayed Fluorescence Process in Carbazole-Benzonitrile Derivatives. *J. Phys. Chem. Lett.* **2019**, *10*, 2475−2480.

(13) de Sa Pereira, D.; Menelaou, C.; Danos, A.; Marian, C.; Monkman, A. P. Electroabsorption Spectroscopy as a Tool for Probing Charge Transfer and State Mixing in Thermally Activated Delayed Fluorescence Emitters. *J. Phys. Chem. Lett.* **2019**, *10*, 3205−3211.

(14) Xue, L.; Cui, B.; Xie, S.; Yin, S. Influence of the Length of the Donor−Acceptor Bridge on Thermally Activated Delayed Fluorescence. *J. Phys. Chem. Lett.* **2019**, *10*, 302−308.

(15) Evans, E. W.; Olivier, Y.; Puttisong, Y.; Myers, W. K.; Hele, T. J. H.; Menke, S. M.; Thomas, T. H.; Credgington, D.; Beljonne, D.; Friend, R. H.; Greenham, N. C. Vibrationally Assisted Intersystem Crossing in Benchmark Thermally Activated Delayed Fluorescence Molecules. *J. Phys. Chem. Lett.* **2018**, *9*, 4053−4058.

(16) Lin, T.-A.; Chatterjee, T.; Tsai, W.-L.; Lee, W.-K.; Wu, M.-J.; Jiao, M.; Pan, K.-C.; Yi, C.-L.; Chung, C.-L.; Wong, K.-T.; Wu, C.-C. Sky-Blue Organic Light Emitting Diode with 37% External Quantum Efficiency Using Thermally Activated Delayed Fluorescence from Spiroacridine-Triazine Hybrid. *Adv. Mater.* **2016**, *28*, 6976−6983.

(17) Wu, T.-L.; Huang, M.-J.; Lin, C.-C.; Huang, P.-Y.; Chou, T.-Y.; Chen-Cheng, R.-W.; Lin, H.-W.; Liu, R.-S.; Cheng, C.-H. Diboron Compound-Based Organic Light-Emitting Diodes with High Efficiency and Reduced Efficiency Roll-Off. *Nat. Photonics* **2018**, *12*, 235−240.

(18) Murawski, C.; Leo, K.; Gather, M. C. Efficiency Roll-Off in Organic Light-Emitting Diodes. *Adv. Mater.* **2013**, *25*, 6801−6827.

(19) Inoue, M.; Serevičius, T.; Nakanotani, H.; Yoshida, K.; Matsushima, T.; Juršėnas, S.; Adachi, C. Effect of Reverse Intersystem Crossing Rate to Suppress Efficiency Roll-off in Organic Light-Emitting Diodes with Thermally Activated Delayed Fluorescence Emitters. *Chem. Phys. Lett.* **2016**, *644*, 62−67.

(20) Tanaka, H.; Shizu, K.; Nakanotani, H.; Adachi, C. Twisted Intramolecular Charge Transfer State for Long-Wavelength Thermally Activated Delayed Fluorescence. *Chem. Mater.* **2013**, *25*, 3766−3771.

(21) Im, Y.; Kim, M.; Cho, Y. J.; Seo, J.-A.; Yook, K. S.; Lee, J. Y. Molecular Design Strategy of Organic Thermally Activated Delayed Fluorescence Emitters. *Chem. Mater.* **2017**, *29*, 1946−1963.

(22) Geng, Y.; D'Aleo, A.; Inada, K.; Cui, L.-S.; Kim, J. U.; Nakanotani, H.; Adachi, C. Donor-*σ*-Acceptor Motifs: Thermally Activated Delayed Fluorescence Emitters with Dual Upconversion. *Angew. Chem., Int. Ed.* **2017**, *56*, 16536−16540.

(23) dos Santos, P. L.; Ward, J. S.; Congrave, D. G.; Batsanov, A. S.; Eng, J.; Stacey, J. E.; Penfold, T. J.; Monkman, A. P.; Bryce, M. R. Triazatruxene: A Rigid Central Donor Unit for a D-A₃ Thermally Activated Delayed Fluorescence Material Exhibiting Sub-Microsecond Reverse Intersystem Crossing and Unity Quantum Yield via Multiple Singlet-Triplet State Pairs. *Adv. Sci.* **2018**, *5*, 1700989.

(24) Wu, K.; Zhang, T.; Zhan, L.; Zhong, C.; Gong, S.; Jiang, N.; Lu, Z.-H.; Yang, C. Optimizing Optoelectronic Properties of Pyrimidine-Based TADF Emitters by Changing the Substituent for Organic Light-Emitting Diodes with External Quantum Efficiency Close to 25% and Slow Efficiency Roll-Off. *Chem. − Eur. J.* **2016**, *22*, 10860−10866.

(25) Komatsu, R.; Sasabe, H.; Nakao, K.; Hayasaka, Y.; Ohsawa, T.; Kido, J. Unlocking the Potential of Pyrimidine Conjugate Emitters to Realize High-Performance Organic Light-Emitting Devices. *Adv. Opt. Mater.* **2017**, *5*, 1600675.

(26) Xiang, Y.; Zhao, Y.; Xu, N.; Gong, S.; Ni, F.; Wu, K.; Luo, J.; Xie, G.; Lu, Z.-H.; Yang, C. Halogen-Induced Internal Heavy-Atom Effect Shortening the Emissive Lifetime and Improving the Fluorescence Efficiency of Thermally Activated Delayed Fluorescence Emitters. *J. Mater. Chem. C* **2017**, *5*, 12204−12210.

(27) Kitamoto, Y.; Namikawa, T.; Ikemizu, D.; Miyata, Y.; Suzuki, T.; Kita, H.; Sato, T.; Oi, S. Light Blue and Green Thermally Activated Delayed Fluorescence from 10H-Phenoxaborin-Derivatives and Their Application to Organic Light-Emitting Diodes. *J. Mater. Chem. C* **2015**, *3*, 9122−9130.

(28) Chen, D.-G.; Lin, T.-C.; Chen, C.-L.; Chen, Y.-T.; Chen, Y.-A.; Lee, G.-H.; Chou, P.-T.; Liao, C.-W.; Chiu, P.-C.; Chang, C.-H.; Lien, Y.-J.; Chi, Y. Optically Triggered Planarization of Boryl-Substituted Phenoxazine: Another Horizon of TADF Molecules and High-Performance OLEDs. *ACS Appl. Mater. Interfaces* **2018**, *10*, 12886−12896.

(29) Liu, Y.; Huang, H.; Zhou, T.; Wu, K.; Zhu, M.; Yu, J.; Xie, G.; Yang, C. Boosting Photoluminescence Quantum Yields of Triarylboron/Phenoxazine Hybrids via Incorporation of Cyano Groups and Their Applications as TADF Emitters for High-Performance Solution-Processed OLEDs. *J. Mater. Chem. C* **2019**, *7*, 4778−4783.

(30) Guo, J.; Fan, J.; Lin, L.; Zeng, J.; Liu, H.; Wang, C.-K.; Zhao, Z.; Tang, B. Z. Mechanical Insights into Aggregation-Induced Delayed Fluorescence Materials with Anti-Kasha Behavior. *Adv. Sci.* **2019**, *6*, 1801629.

(31) Xiang, Y.; Zhu, Z.-L.; Xie, D.; Gong, S.; Wu, K.; Xie, G.; Lee, C.-S.; Yang, C. Revealing the New Potential of an Indandione Unit for Constructing Efficient Yellow Thermally Activated Delayed Fluorescence Emitters with Short Emissive Lifetimes. *J. Mater. Chem. C* **2018**, *6*, 7111−7118.

(32) Chen, Z.; Wu, Z.; Ni, F.; Zhong, C.; Zeng, W.; Wei, D.; An, K.; Ma, D.; Yang, C. Emitters with a Pyridine-3,5-Dicarbonitrile Core and Short Delayed Fluorescence Lifetimes of about 1.5 Ms: Orange-Red TADF-Based OLEDs with Very Slow Efficiency Roll-Offs at High Luminance. *J. Mater. Chem. C* **2018**, *6*, 6543−6548.

(33) Cai, X.; Su, S.-J. Marching Toward Highly Efficient, Pure-Blue, and Stable Thermally Activated Delayed Fluorescent Organic Light-Emitting Diodes. *Adv. Funct. Mater.* **2018**, *28*, 1802558.

(34) Wang, K.; Zheng, C.-J.; Liu, W.; Liang, K.; Shi, Y.-Z.; Tao, S.-L.; Lee, C.-S.; Ou, X.-M.; Zhang, X.-H. Avoiding Energy Loss on TADF Emitters: Controlling the Dual Conformations of D-A Structure Molecules Based on the Pseudoplanar Segments. *Adv. Mater.* **2017**, *29*, 1701476.

(35) Chen, C.; Huang, R.; Batsanov, A. S.; Pander, P.; Hsu, Y.-T.; Chi, Z.; Dias, F. B.; Bryce, M. R. Intramolecular Charge Transfer Controls Switching Between Room Temperature Phosphorescence and Thermally Activated Delayed Fluorescence. *Angew. Chem.* **2018**, *57*, 16407−16411.

(36) Wang, K.; Shi, Y.-Z.; Zheng, C.-J.; Liu, W.; Liang, K.; Li, X.; Zhang, M.; Lin, H.; Tao, S.-L.; Lee, C.-S.; Ou, X.-M.; Zhang, X.-H. Control of Dual Conformations: Developing Thermally Activated Delayed Fluorescence Emitters for Highly Efficient Single-Emitter White Organic Light-Emitting Diodes. *ACS Appl. Mater. Interfaces* **2018**, *10*, 31515−31525.

(37) Serevičius, T.; Skaisgiris, R.; Dodonova, J.; Jagintavičius, L.; Bucevičius, J.; Kazlauskas, K.; Juršėnas, S.; Tumkevičius, S. Emission Wavelength Dependence on rISC Rate in TADF Compounds with Large Conformational Disorder. *Chem. Commun.* **2019**, *55*, 1975−1978.

(38) Kretzschmar, A.; Patze, C.; Schwaebel, S. T.; Bunz, U. H. F. Development of Thermally Activated Delayed Fluorescence Materials with Shortened Emissive Lifetimes. *J. Org. Chem.* **2015**, *80*, 9126−9131.

(39) Rothe, C.; Monkman, A. P. Triplet Exciton Migration in a Conjugated Polyfluorene. *Phys. Rev. B* **2003**, *68*, No. 075208.

(40) de Mello, J. C.; Wittmann, H. F.; Friend, R. H. An Improved Experimental Determination of External Photoluminescence Quantum Efficiency. *Adv. Mater.* **1997**, *9*, 230−232.

(41) Komatsu, R.; Ohsawa, T.; Sasabe, H.; Nakao, K.; Hayasaka, Y.; Kido, J. Manipulating the Electronic Excited State Energies of Pyrimidine-Based Thermally Activated Delayed Fluorescence Emitters To Realize Efficient Deep-Blue Emission. *ACS Appl. Mater. Interfaces* **2017**, *9*, 4742−4749.

(42) Cui, L.-S.; Nomura, H.; Geng, Y.; Kim, J. U.; Nakanotani, H.; Adachi, C. Controlling Singlet-Triplet Energy Splitting for Deep-Blue Thermally Activated Delayed Fluorescence Emitters. *Angew. Chem., Int. Ed.* **2017**, *56*, 1571−1575.

(43) Oh, C. S.; Han, S. H.; Lee, J. Y. Molecular Design of Thermally Activated Delayed Fluorescent Emitters for Blue-Shifted Emission by Methoxy Substitution. *J. Mater. Chem. C* **2017**, *5*, 9106−9114.

(44) Huang, W.; Einzinger, M.; Maurano, A.; Zhu, T.; Tiepelt, J.; Yu, C.; Chae, H. S.; Van Voorhis, T.; Baldo, M. A.; Buchwald, S. L. Large Increase in External Quantum Efficiency by Dihedral Angle Tuning in a Sky-Blue Thermally Activated Delayed Fluorescence Emitter. *Adv. Opt. Mater.* **2019**, *7*, 1900476.

(45) Wu, T.-L.; Lo, S.-H.; Chang, Y.-C.; Huang, M.-J.; Cheng, C.-H. Steric Switching for Thermally Activated Delayed Fluorescence by Controlling the Dihedral Angles between Donor and Acceptor in Organoboron Emitters. *ACS Appl. Mater. Interfaces* **2019**, *11*, 10768−10776.

(46) Woo, S.-J.; Kim, Y.; Kwon, S.-K.; Kim, Y.-H.; Kim, J.-J. Phenazasiline/Spiroacridine Donor Combined with Methyl-Substituted Linkers for Efficient Deep Blue Thermally Activated Delayed Fluorescence Emitters. *ACS Appl. Mater. Interfaces* **2019**, *11*, 7199−7207.

(47) Frisch, M. J.; Trucks, G. W.; Schlegel, H. B.; Scuseria, G. E.; Robb, M. A.; Cheeseman, J. R.; Scalmani, G.; Barone, V.; Mennucci, B.; Petersson, G. A.; Nakatsuji, H.; Caricato, M.; Li, X.; Hratchian, H. P.; Izmaylov, A. F.; Bloino, J.; Zheng, G.; Sonnenberg, J. L.; Hada, M.; Ehara, M.; Toyota, K.; Fukuda, R.; Hasegawa, J.; Ishida, M.; Nakajima, T.; Honda, Y.; Kitao, O.; Nakai, H.; Vreven, T.; Montgomery, Jr., J. A.; Peralta, J. E.; Ogliaro, F.; Bearpark, M.; Heyd, J. J.; Brothers, E.; Kudin, K. N.; Staroverov, V. N.; Keith, T.; Kobayashi, R.; Normand, J.; Raghavachari, K.; Rendell, A.; Burant, J. C.; Iyengar, S. S.; Tomasi, J.; Cossi, M.; Rega, N.; Millam, J. M.; Klene, M.; Knox, J. E.; Cross, J. B.; Bakken, V.; Adamo, C.; Jaramillo, J.; Gomperts, R.; Stratmann, R. E.; Yazyev, O.; Austin, A. J.; Cammi, R.; Pomelli, C.; Ochterski, J. W.; Martin, R. L.; Morokuma, K.; Zakrzewski, V. G.; Voth, G. A.; Salvador, P.; Dannenberg, J. J.; Dapprich, S.; Daniels, A. D.; Farkas, O.; Foresman, J. B.; Ortiz, J. V.; Cioslowski, J.; Fox, D. J. *Gaussian 09*; Revision C.01, Gaussian, Inc.: Wallingford CT, 2010.

(48) Peng, Q.; Fan, D.; Duan, R.; Yi, Y.; Niu, Y.; Wang, D.; Shuai, Z. Theoretical Study of Conversion and Decay Processes of Excited Triplet and Singlet States in a Thermally Activated Delayed Fluorescence Molecule. *J. Phys. Chem. C* **2017**, *121*, 13448−13456.

(49) Wang, L.; Cai, X.; Li, B.; Li, M.; Wang, Z.; Gan, L.; Qiao, Z.; Xie, W.; Liang, Q.; Zheng, N.; Liu, K.; Su, S.-J. Achieving Enhanced Thermally Activated Delayed Fluorescence Rates and Shortened Exciton Lifetimes by Constructing Intramolecular Hydrogen Bonding Channels. *ACS Appl. Mater. Interfaces* **2019**, *11*, 45999−46007.

(50) Cotts, B. L.; McCarthy, D. G.; Noriega, R.; Penwell, S. B.; Delor, M.; Devore, D. D.; Mukhopadhyay, S.; De Vries, T. S.; Ginsberg, N. S. Tuning Thermally Activated Delayed Fluorescence Emitter Photophysics through Solvation in the Solid State. *ACS Energy Lett.* **2017**, *2*, 1526−1533.

(51) Kim, J. H.; Yun, J. H.; Lee, J. Y. Recent Progress of Highly Efficient Red and Near-Infrared Thermally Activated Delayed Fluorescent Emitters. *Adv. Opt. Mater.* **2018**, *6*, 1800255.

(52) Kreiza, G.; Banevičius, D.; Jovaišaitė, J.; Maleckaitė, K.; Gudeika, D.; Volyniuk, D.; Gražulevičius, J. V.; Juršėnas, S.; Kazlauskas, K. Suppression of Benzophenone-Induced Triplet Quenching for Enhanced TADF Performance. *J. Mater. Chem. C* **2019**, *7*, 11522−11531.

(53) Köhler, A.; Bässler, H. Triplet States in Organic Semiconductors. *Mater. Sci. Eng. R Rep.* **2009**, *66*, 71−109.

(54) Ward, J. S.; Nobuyasu, R. S.; Batsanov, A. S.; Data, P.; Monkman, A. P.; Dias, F. B.; Bryce, M. R. The Interplay of Thermally Activated Delayed Fluorescence (TADF) and Room Temperature Organic Phosphorescence in Sterically-Constrained Donor−Acceptor Charge-Transfer Molecules. *Chem. Commun.* **2016**, *52*, 2612−2615.

(55) Dias, F. B.; Penfold, T. J.; Monkman, A. P. Photophysics of Thermally Activated Delayed Fluorescence Molecules. *Methods Appl. Fluoresc.* **2017**, *5*, No. 012001.

(56) Serevičius, T.; Bučiūnas, T.; Bucevičius, J.; Dodonova, J.; Tumkevičius, S.; Kazlauskas, K.; Juršėnas, S. Room Temperature Phosphorescence *vs.* Thermally Activated Delayed Fluorescence in Carbazole−Pyrimidine Cored Compounds. *J. Mater. Chem. C* **2018**, *6*, 11128−11136.

(57) Etherington, M. K.; Franchello, F.; Gibson, J.; Northey, T.; Santos, J.; Ward, J. S.; Higginbotham, H. F.; Data, P.; Kurowska, A.; Dos Santos, P. L.; Graves, D. R.; Batsanov, A. S.; Dias, F. B.; Bryce, M. R.; Penfold, T. J.; Monkman, A. P. Regio- and Conformational Isomerization Critical to Design of Efficient Thermally-Activated Delayed Fluorescence Emitters. *Nat. Commun.* **2017**, *8*, 14987.

(58) Northey, T.; Stacey, J.; Penfold, T. J. The Role of Solid State Solvation on the Charge Transfer State of a Thermally Activated Delayed Fluorescence Emitter. *J. Mater. Chem. C* **2017**, *5*, 11001−11009.

(59) Weissenseel, S.; Drigo, N. A.; Kudriashova, L. G.; Schmid, M.; Morgenstern, T.; Lin, K.-H.; Prlj, A.; Corminboeuf, C.; Sperlich, A.; Brütting, W.; Nazeeruddin, M. K.; Dyakonov, V. Getting the Right Twist: Influence of Donor−Acceptor Dihedral Angle on Exciton Kinetics and Singlet−Triplet Gap in Deep Blue Thermally Activated Delayed Fluorescence Emitter. *J. Phys. Chem. C* **2019**, *123*, 27778−27784.

(60) Wada, Y.; Kubo, S.; Kaji, H. Adamantyl Substitution Strategy for Realizing Solution-Processable Thermally Stable Deep-Blue Thermally Activated Delayed Fluorescence Materials. *Adv. Mater.* **2018**, *30*, 1705641.

(61) Wada, Yoshimasa; Nakagawa, H.; Matsumoto, S.; Wakisaka, Y.; Kaji, H. Molecular Design Realizing Very Fast Reverse Intersystem Crossing in Purely Organic Emitter. 2019, *ChemRxiv*: doi.org/10.26434/chemrxiv.9745289.v1 ChemRxiv.org e-Print archive preprint. https://chemrxiv.org/articles/Molecular_Design_Realizing_Very_Fast_Reverse_Intersystem_Crossing_in_Purely_Organic_Emitter/9745289/1 (accessed Nov. 21, 2019).

(62) Liu, Y.; Li, C.; Ren, Z.; Yan, S.; Bryce, M. R. All-Organic Thermally Activated Delayed Fluorescence Materials for Organic Light-Emitting Diodes. *Nat. Rev. Mater.* **2018**, *3*, 18020.

(63) Tsai, Y.-S.; Hong, L.-A.; Juang, F.-S.; Chen, C.-Y. Blue and White Phosphorescent Organic Light Emitting Diode Performance Improvement by Confining Electrons and Holes inside Double Emitting Layers. *J. Lumin.* **2014**, *153*, 312−316.

(64) Srivastava, R.; Joshi, L. R. The Effect of Substituted 1,2,4-Triazole Moiety on the Emission, Phosphorescent Properties of the Blue Emitting Heteroleptic Iridium(III) Complexes and the OLED Performance: A Theoretical Study. *Phys. Chem. Chem. Phys.* **2014**, *16*, 17284−17294.

(65) Chatterjee, T.; Wong, K.-T. Perspective on Host Materials for Thermally Activated Delayed Fluorescence Organic Light Emitting Diodes. *Adv. Opt. Mater.* **2019**, *7*, 1800565.

(66) Zhang, J.; Ding, D.; Wei, Y.; Xu, H. Extremely Condensing Triplet States of DPEPO-Type Hosts through Constitutional Isomerization for High-Efficiency Deep-Blue Thermally Activated Delayed Fluorescence Diodes. *Chem. Sci.* **2016**, *7*, 2870−2882.

(67) Gather, M. C.; Reineke, S. Recent Advances in Light Outcoupling from White Organic Light-Emitting Diodes. *J. Photon. Energy* **2015**, *5*, No. 057607.

(68) Liu, M.; Komatsu, R.; Cai, X.; Hotta, K.; Sato, S.; Liu, K.; Chen, D.; Kato, Y.; Sasabe, H.; Ohisa, S.; Suzuri, Y.; Yokoyama, D.; Su, S.-J.; Kido, J. Horizontally Orientated Sticklike Emitters: Enhancement of Intrinsic Out-Coupling Factor and Electroluminescence Performance. *Chem. Mater.* **2017**, *29*, 8630−8636.

(69) Ihn, S.-G.; Lee, N.; Jeon, S. O.; Sim, M.; Kang, H.; Jung, Y.; Huh, D. H.; Son, Y. M.; Lee, S. Y.; Numata, M.; Miyazaki, H.; Gómez-Bombarelli, R.; Aguilera-Iparraguirre, J.; Hirzel, T.; Aspuru-Guzik, A.; Kim, S.; Lee, S. An Alternative Host Material for Long-Lifespan Blue Organic Light-Emitting Diodes Using Thermally Activated Delayed Fluorescence. *Adv. Sci.* **2017**, *4*, 1600502.